FSI-06-TN75

THREE-DIMENSIONAL COLLISION MODELING FOR RIGID BODIES AND ITS COUPLING WITH FLUID FLOW COMPUTATION

Gengsheng Wei
Flow Science, Inc.
March, 2006

A computational algorithm for 3-D rigid-body collision and its coupling with fluid flow was developed and implemented in ***FLOW-3D***® as an addition to the existing General Moving Object (GMO) model. It is assumed that all the bodies have negligible deformation during collision and instantaneously change velocities when they collide. A set of existing equations of motion for collision under six degrees of freedom were adopted. Modifications were made for collisions of bodies with fixed axis, fixed point and prescribed motion. Numerical methods for collision detection and collision integration were developed. Stronge's energetic coefficient of restitution was employed to determine completion of collision calculation. The model allows for simultaneous collisions of multiple bodies. Collisions can be perfectly elastic, partially plastic or completely plastic. Surfaces of bodies can be smooth or rough, allowing existence of impulse of friction during collision. Continuous contact between moving objects is modeled through a series of micro-collisions. Several applications of the model with and without presence of fluid flow were made. Good agreements of the computational results with analytical and experimental results were obtained and are presented at the end of the report.

1. Introduction

A fixed-mesh method for general moving objects in fluid flow (named GMO model) was developed and released in a previous version of ***FLOW-3D***® (Wei, 2005a, 2005b, Barkhudarov and Wei, 2006). A general moving object is a rigid body with any type of motion which is either user-prescribed (prescribed motion) or dynamically coupled to fluid flow (coupled motion). The method allows for multiple general moving objects in one problem, each of which can be assigned any prescribed or couple motion with 6 DOF, fixed axis or fixed point. At each time step, area and volume fractions in a fixed-rectangular mesh are calculated to describe the object's motion. Hydraulic, gravitational, environmental, non-inertial and residual control forces and torques are calculated for each moving object. Equations of motion are solved for translational and rotational velocities for objects under coupled motion. Several aspects make the fixed mesh method superior to the more conventional moving mesh, deforming mesh and re-meshing methods: it is more computationally efficient due to no adjustment and regeneration of mesh; it does not need repeated flow field interpolation which can accumulate computational error and possibly ruin the computational result; it imposes no limitation on the distance between moving objects.

In applications of CFD, there are many cases which require simulation of rigid body collision, e.g., a berthing ship impacting on a fendered dock, wood logs and debris hitting on a structure when they are drifted by flooding water, and a during closing of a valve. The first release of the GMO model possessed no collision capability. When moving bodies collide on each other or hit a solid wall, there is no contact force to prevent them from overlapping. The bodies thus go through each other or penetrate into the solid walls.

In this work the capability to simulate rigid body collision was developed for ***FLOW-3D***®. The model of Stronge (Stronge, 2000) for collision with six degrees of freedom (DOF) was adopted. It was further modified for two more cases: 1) colliding bodies with fixed axis/point, 2) in a pair of colliding bodies one has prescribed motion and the other has coupled motion. Numerical algorithm for collision detection and collision integration were also developed and incorporated into the code. The collision model is compatible with the original GMO model. In a multiple body system, different bodies can possess different types of prescribed and coupled motions, and simultaneous collisions of multiple moving bodies are allowed. Collisions can also occur between moving bodies and wall or symmetric boundaries of the computational domain. Collisions can be perfectly elastic, partially plastic or completely plastic. Object surfaces can be smooth or rough, allowing existence of friction at the point of contact during collision. There can be relative sliding between two colliding bodies at their contact point and the speed and direction of sliding can vary throughout the collision process. If sliding stops before collision is competed, the two bodies can either stick or resume sliding immediately until they are separated. Continuous contact between moving objects, such as sliding, rolling and sitting of one body on the other, is modeled through a series of rapid collisions, called micro-collisions. Limitations exist for the collision model. When an object collides simultaneously with multiple objects, the collision dynamics is approximated by splitting it into a number of sub-collisions between the object and each of the others. The order of the sub-collisions may to some degree affect the total result. Another weakness of the model is that when one object continuously sits on another, mutual penetration of the two objects may occur if micro-collision is partially plastic and the time step for fluid flow integration is relatively large.

This report presents the equations of motion, the treatment of friction, the algorithms for collision detection and integration, the formation of the collision reference system and its transformation to space and body-fitted systems. Computational results of several application cases are presented, together with comparisons with analytical and experimental results. These cases include solid sphere collision, pool ball breaking, domino toppling, drifting of logs by water through a reservoir gate, flushing of a spherical object in a toilet, and transport of stones by water stream in a stepped channel.

2. Equations of Motion for Collision

2.1 Assumptions

It is assumed that all the bodies are rigid, i.e., their deformation during collision are negligible and they instantaneously change velocities when they collide. Friction can exist during collision for bodies with rough surfaces based on Coulomb's Law of friction. Stronge's energetic coefficient of restitution is utilized to determine the completion of the collision integration. Newton's law for impact and Possion's hypothesis for collision are not adopted in this model because they can cause energy increase when friction is present (Mirtich, 1996, Stronge, 2000).

2.1.1 Coulomb's Law of friction

Assume body B collides on body B' and their contact point (or collision point) is respectively denoted as C on body B and C' on body B'. A collision reference system (collision system) is set up with its origin located at the contact point with $\mathbf{n}_1$, $\mathbf{n}_2$, $\mathbf{n}_3$ denoting the unit vectors of its three coordinate axes. $\mathbf{n}_3$ is along the normal direction of the common tangential plane of the two bodies at the contact point and its direction points from body B' to body B. Let $\vec{v}$ represent the velocity of point C relative to C', and $\vec{p}$ the impulse of the contact force on body B. In vector form, they are

$$\vec{v} = (v_1, v_2, v_3), \ \vec{p} = (p_1, p_2, p_3) \tag{1}$$

where the lower index represents the corresponding component along the $\mathbf{n}_1$, $\mathbf{n}_2$ and $\mathbf{n}_3$ axes. We now simply denote $\mathbf{n}$ for the normal direction $\mathbf{n}_3$ and p for the normal impulse p_3, Coulomb's law of friction is then written as

$$\sqrt{(dp_1)^2 + (dp_2)^2} < \mu\, dp, \qquad \text{if } \ v_1^{\,2} + v_2^{\,2} = 0 \tag{2}$$

$$dp_i = -\frac{\mu v_i}{\sqrt{v_1^{\,2} + v_2^{\,2}}} dp, \quad i = 1, 2, \quad \text{if } v_1^{\,2} + v_2^{\,2} > 0 \tag{3}$$

Equation (3) can also be written as

$$dp_1 = -\mu \cos\phi \ dp, \ \ dp_2 = -\mu \sin\phi \, dp, \quad \text{if } v_1^{\,2} + v_2^{\,2} > 0 \tag{4}$$

where ϕ is the angle of the sliding direction measured from $\mathbf{n}_1$ about **n.**

2.1.2 Stronge's energetic coefficient of restitution

As generally understood, a collision process is divided into the compression and restitution phases. Stronge's hypothesis is to relate the work done by normal impulse during restitution to that during compression. Stronge's energetic coefficient of restitution e_* is defined

$$e^2 = -\frac{W_3(p_f) - W_3(p_c)}{W_3(p_c)}, \tag{5}$$

where W_3 is the work done by the normal impulse, p_c is the normal impulse when collision reaches maximum compression, and p_f is the total impulse of the collision. In (5), the numerator is the total work by normal impulse during restitution and is always nonnegative, and the denominator is that during compression and is always negative. Stronge's hypothesis is that the collision is completed when (5) is satisfied. The value of e is 1 for purely elastic collision, 0 for completely plastic collision, and between 0 and 1 for partially elastic collision. W_3 is calculated by

$$W_3(p) = \int_0^p v_3 dp \tag{6}$$

2.2. Equations of Motion in General Form

Assume the two bodies B and B' illustrated in section 2.2.1 have mass M and M', and their mass centers are located at G and G', respectively. In the collision system, the relative velocity $\vec{v}$ at the contact point satisfies the equation of motion (Stronge, 2000),

$$dv_i = m_{ij}^{-1} dp_j \qquad (i=1,2,3) \tag{7}$$

where Einstein's convention of summation is used, and

$$m_{ij}^{-1} = m_{B,ij}^{-1} + m_{B',ij}^{-1} \tag{8}$$

in which $m_{B,ij}^{-1}$ and $m_{B',ij}^{-1}$ are terms for bodies B and B', respectively. If both bodies have 6 DOF, the expressions of $m_{B,ij}^{-1}$ and $m_{B',ij}^{-1}$ are

$$m_{B,ij}^{-1} = \frac{1}{M}\delta_{ij} + \varepsilon_{ikm}\varepsilon_{jln}J_{kl}^{-1}r_m r_n \qquad \text{(6 DOF)} \tag{9}$$

$$m_{B',ij}^{-1} = \frac{1}{M'}\delta_{ij} + \varepsilon_{ikm}\varepsilon_{jln}J_{kl}'^{-1}r_m' r_n' \qquad \text{(6 DOF)} \tag{10}$$

where δ_{ij} is Kronecker delta, ε_{ijk} is permutation tensor, J_{kl}^{-1} and $J_{kl}'^{-1}$ are elements of the respective inverse inertia tensors about mass centers for the two bodies in the collision system, r_i and r_i' the components of the respective distance vectors from the mass centers to the collision point for the two bodies.

In this work, derivations were also made for $m_{B,ij}^{-1}$ for a rigid body under fixed-axis or fixed-point coupled motions. For the fixed-point case, $m_{B,ij}^{-1}$ is

$$m_{B,ij}^{-1} = \varepsilon_{ikm}\varepsilon_{jln}J_{kl}^{-1}r_m r_n \qquad \text{(fixed-point)} \tag{11}$$

where J_{ij}^{-1} represents the inverse inertia tensor about the fixed point in the collision system, r_i are the components of the distance vector from the fixed point to the collision point. For body with fixed axis,

$$m_{B,ij}^{-1} = A_{il}B_{lj} \qquad \text{(fixed-axis)} \tag{12}$$

where index l is not a dummy index but the denotation of the rotation orientation: l is equal to 1, 2 or 3 for the rotation axis parallel to x, y or z of the space coordinate system, respectively. A_{il} and B_{lj} are

$$A_{il} = R_{im}\varepsilon_{mlk}r_k^s \tag{13}$$

$$B_{lj} = \frac{1}{J_{ll}^s}\varepsilon_{lnq}r_n^s R_{jq} \tag{14}$$

where J_{ll}^s is the moment of inertia about the rotation axis in space system, r_n^s are the components of the distance vector in the space system from an arbitrary point on the rotation axis to the collision point, R_{jq} are the elements of the coordinate transformation tensor from the space system to the collision system $[R]_{cs}$, which will be discussed in section 2.4. Expressions of $m_{B',ij}^{-1}$ are similar to (11) to (14) with the corresponding variables replaced by those for object B'.

When the two colliding objects have different types of coupled motion (e.g., one has 6 DOF and the other fixed-axis), $m_{B,ij}^{-1}$ and $m_{B',ij}^{-1}$ are different in expressions selected from (10) to (13). If one colliding object is stationary or has prescribed motion, its corresponding term $m_{B,ij}^{-1}$ or $m_{B',ij}^{-1}$ is equal to zero.

2.3. Equations of Motion in Terms of Normal Impulse

If two bodies in collision slide initially at their contact point, then friction may bring slip to a halt when collision is eccentric and initial speed of sliding is small enough. An eccentric collision means that the mass centers of the two colliding bodies and the collision point are not along the same line. After the halt occurs, the two bodies either stick at the contact point (called slip-stick) or renew sliding immediately (called slip reversal) in a new direction until they are separated, depending on the inertia properties of the two objects and the friction coefficient. The sliding before the halt occurs is called the first phase of sliding, and slip reversal is called the second phase of sliding. If friction does not cause a halt of the slip or the collision is frictionless, only the first phase of sliding can exist throughout collision.

2.3.1. First Phase of Sliding

When two objects slide during collision, the tangential velocity components are

$$v_1 = s\cos\phi\,,\ v_2 = s\sin\phi\,, \tag{15}$$

where s is sliding speed,

$$s = \sqrt{{v_1}^2 + {v_2}^2} \tag{16}$$

and ϕ is the sliding direction which varies during collision. Introducing Coulomb's Law of friction (4) into equation (7), equations of motion in terms of the normal impulse p for the first phase of sliding are (Stronge, 2000)

$$\frac{dv_1}{dp} = -\mu m_{11}^{-1}\cos\phi - \mu m_{12}^{-1}\sin\phi + m_{13}^{-1} \tag{17}$$

$$\frac{dv_2}{dp} = -\mu m_{21}^{-1}\cos\phi - \mu m_{22}^{-1}\sin\phi + m_{23}^{-1} \tag{18}$$

$$\frac{dv_3}{dp} = -\mu m_{31}^{-1}\cos\phi - \mu m_{32}^{-1}\sin\phi + m_{33}^{-1} \tag{19}$$

If the objects are perfectly smooth ($\mu = 0$), then (17) to (19) are independent of each other, otherwise they are coupled. Equations governing s and ϕ are (Keller, 1986, Stronge, 2000)

$$\frac{ds}{dp} = m_{13}^{-1}\cos\phi + m_{23}^{-1}\sin\phi - \mu m_{11}^{-1}\cos^2\phi - 2\mu m_{12}^{-1}\sin\phi\cos\phi - \mu m_{22}^{-1}\sin^2\phi \equiv g(\mu,\phi) \tag{20}$$

$$s\frac{d\phi}{dp} = -m_{13}^{-1}\sin\phi + m_{23}^{-1}\cos\phi + \mu(m_{11}^{-1} - m_{22}^{-1})\sin\phi\cos\phi + \mu m_{12}^{-1}(\sin^2\phi - \cos^2\phi) \equiv h(\mu,\phi) \tag{21}$$

2.3.2. Slip-Stick

During slip-stick, $v_1 = v_2 = 0$ and $dv_1/dp = dv_2/dp = 0$. The zero tangential velocity is accompanied by a tangential frictional force along a constant direction $\bar{\phi} - \pi$. It is shown that (Stronge, 2000)

$$\bar{\phi} = \tan^{-1}\left(\frac{m_{11}^{-1} m_{23}^{-1} - m_{12}^{-1} m_{13}^{-1}}{m_{22}^{-1} m_{13}^{-1} - m_{23}^{-1} m_{12}^{-1}} \right) \tag{22}$$

Components of the differential impulse of the tangential force in $\mathbf{n_1}$ and $\mathbf{n_2}$ satisfy

$$dp_1 = -\bar{\mu} \cos\bar{\phi}\ dp\,, \quad dp_2 = -\bar{\mu} \sin\bar{\phi}\ dp \tag{23}$$

$$\sqrt{(dp_1)^2 + (dp_2)^2} = \bar{\mu}\, dp \tag{24}$$

where $\bar{\mu}$ is the coefficient of stick,

$$\bar{\mu} = \frac{\sqrt{(m_{11}^{-1} m_{23}^{-1} - m_{12}^{-1} m_{13}^{-1})^2 + (m_{22}^{-1} m_{13}^{-1} - m_{23}^{-1} m_{12}^{-1})^2}}{m_{11}^{-1} m_{22}^{-1} - m_{12}^{-1} m_{12}^{-1}} \tag{25}$$

and $\bar{\mu} < \mu$. Equations of motion thus are

$$v_1 = 0 \tag{26}$$

$$v_2 = 0 \tag{27}$$

$$\frac{dv_3}{dp} = -\bar{\mu}\, m_{31}^{-1} \cos\bar{\phi} - \bar{\mu}\, m_{32}^{-1} \sin\bar{\phi} + m_{33}^{-1} \tag{28}$$

2.3.3. Second Phase of Sliding (slip reversal)

During the second phase of sliding, or slip reversal, equations of motion (17) to (19) are still valid. However, different from the first phase of sliding in which sliding direction varies during collision, sliding in the second phase is along a constant direction ϕ. It is obtained by solving $h(\mu, \phi) = 0$ in (21) for ϕ. There can be multiple solutions for ϕ. The sliding direction is the unique solution satisfying $ds/dp = g(\mu, \phi) > 0$ defined in equation (20).

2.3.4 Criterion for Slip Stick and Slip Reversal

If friction causes slip halt, then comparison of the friction coefficient μ and the coefficient of stick $\bar{\mu}$ determines if slip stick or slip reversal occurs after that. If $\bar{\mu} < \mu$, slip-stick is achieved. Otherwise, slip reversal happens immediately.

2.3.4. Velocity of object after separation

Once the Stronge's hypothesis in (5) is satisfied, collision integration ends and the two bodies B and B' are separated. The mass center velocity and the angular velocity of B after collision are obtained through an integrated form of the equation of motion in terms of the total impulse. For 6-DOF motion, they are

$$\vec{V}_G = \vec{V}_{G,0} + \frac{\vec{p}}{M}, \tag{29}$$

$$\vec{\omega} = \vec{\omega}_0 + [J]^{-1} \cdot [\vec{r} \times \vec{p}], \tag{30}$$

where $\vec{V}_{G,0}$ and $\vec{\omega}_0$ are respectively the mass center velocity and the angular velocity before the collision, M is the mass, $\vec{r}$ is the distance vector from the mass center G to the collision point C, and $\vec{p}$ is the total impulse at the end of collision,

$$\vec{p} = p_1\vec{n}_1 + p_2\vec{n}_2 + p_3\vec{n}_3. \tag{31}$$

Equation (29) is in the space system, whereas equation (30) can be either in space or body-fitted systems. The mass center and the angular velocities of object B' are calculated in the same way as those of B. Note that the impulse acting on B' is equal in magnitude, but opposite in direction to that on B. For the fixed-axis and fixed-point motions, the integrated forms of the equation of motion are easily obtained and not presented here.

2.4 Formation of Collision Reference System and Coordinate Transformation

In this work, a method to form a collision reference system is proposed and its transformation equations to other reference systems are presented. As presented in the previous sections, the collision system has its origin located at the contact point, and the third coordinate axis $\vec{n}_3$ is along the common direction normal to the surface at the contact point. Definitions of the other two coordinate axes $\vec{n}_1$ and $\vec{n}_2$ are illustrated in Figure 1. Let O be the origin of the space system (x, y, z). Line OB is along the direction of $\vec{n}_3$ and forms angle θ with z axis. The projection of $\vec{n}_3$ in x-y plane forms angle β with x axis. Denote the normal direction of the plane formed by z axis and OB as OD. Now we rotate the space coordinate system about OD for angle β, and the new positions of x, y and z axes denoted are as OX', OY' and OZ', respectively. OX', OY' and OZ' are defined as the directions of the coordinate axes $\vec{n}_1$, $\vec{n}_2$ and $\vec{n}_3$ of the collision system. This method guarantees that a 2-D problem in space system remains 2-D in the collision system and treatments for 2-D and 3-D problems are consistent.

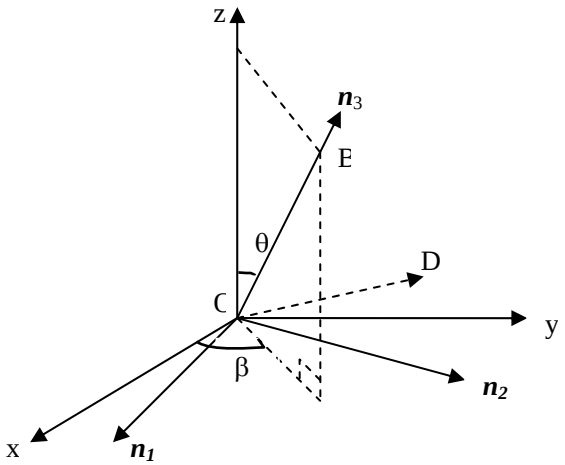

Figure 1. Illustration of the formation of the collision system

When this collision model is incorporated into the existing GMO model, we use three reference systems: the collision system, the space system and the body-fitted system. Transformations between different reference systems are needed. Let a vector $\vec{A}$ be written as $\vec{A}_C$, $\vec{A}_S$ and $\vec{A}_B$ in the collision, space and body systems, respectively. The equations for transformation of $\vec{A}$ between any two of these systems are

$$\vec{A}_S = [R]_{SB}\,\vec{A}_B\,, \tag{32}$$

$$\vec{A}_C = [R]_{CS}\,\vec{A}_S\,, \tag{33}$$

$$\vec{A}_C = [R]_{CB}\,\vec{A}_B\,, \tag{34}$$

For a 3×3 tensor, e.g., the moment of inertia tensor [*J*], its transformation between the body-fitted and the collision systems is

$$[J]_C = [R]_{CB} \cdot [J]_B \cdot [R]_{CB}^T \tag{35}$$

where $[J]_B$ and $[J]_C$ are in the body-fitted and the collision systems, respectively, $[R]_{SB}$, $[R]_{CS}$ and $[R]_{CB}$ are transformation tensors, and

$$[R]_{CB} = [R]_{CS}[R]_{SB} \tag{36}$$

In the existing GMO model, there is calculation of the transformation tensor $[R]_{SB}$ already. Thus, if we know $[R]_{CS}$, then $[R]_{CB}$ can be calculated using (35) and transformation of any vector and tensor between any two systems can be made. Derivation shows that

$$[R]_{CS} = \begin{bmatrix} \sin^2\beta + \cos^2\beta\cos\theta & -\sin\beta\cos\beta(1-\cos\theta) & -\cos\beta\sin\theta \\ -\sin\beta\cos\beta(1-\cos\theta) & \cos^2\beta + \sin^2\beta\cos\theta & -\sin\beta\sin\theta \\ \cos\beta\sin\theta & \sin\beta\sin\theta & \cos\theta \end{bmatrix} \tag{37}$$

It is noted that the transformation tensors are orthogonal and satisfies $[R]^T \equiv [R]^{-1}$, where $[R]^T$ and $[R]^{-1}$ are transpose and inverse of [R], respectively.

3. Numerical Algorithms and Code Implementation

At each time step for the fluid flow computation, the collision calculation is conducted following two steps: collision detection and collision integration. Collision detection checks whether two bodies collide and calculates the location of the contact point. It is conducted for all possible combinations of two bodies, at least one of which must be a moving body. It is also made between moving bodies and wall/symmetric boundaries of the computational domain (collision with a symmetric boundary is always frictionless and purely elastic). Collision integration is conducted once collision is confirmed and a contact point is found. It solves the equations of motion for collision and gives the total impulse and the translational and rotational velocities of the colliding bodies at the end of the collision process.

3.1 Collision Detection

For any two bodies, collision detection checks whether: 1) an overlap is formed between them, and 2) the component of the relative velocity along their common normal direction of surface at the contact point is negative. If both conditions are satisfied, then collision is confirmed and the location of the collision point is calculated. In this work, the collision detection technique is unique. It is based on the FAVOR method and balanced in efficiency and accuracy of the computation. It works for objects defined by both STL data and quadratic functions.

In the preprocessor, all boundary cells of fixed and moving bodies are searched and their parameters are calculated for input to the solver. A boundary cell of a body is either a mesh cell intersected by the surface of the body or a mesh cell completely inside the body with at least one neighbor mesh cell completely outside the body. The surface parameters of a boundary cell include the normal direction to the body surface and the location of a point on the body surface inside this boundary cell. In the solver, boundary cells and their parameters are updated at each time step only for moving bodies. Currently, it is assumed that the collision point is at a grid node overlapped by both colliding bodies. Collision detection is conducted with the following steps:

1) Check if the two bodies have a common boundary cell. If yes, find the mesh corner points inside both objects.
2) Compare all the common boundary cells to find the grid node with negative relative velocity along the normal direction and the largest normal distance to the two object surfaces.
3) If a point in step 2) is found, then collision is confirmed and that point is selected as the contact point.
4) Surface curvature is compared for the two bodies around the contact point. The normal direction of the body surface with the smallest curvature is selected as the common normal direction of the two bodies at the contact point.

3.2 Collision Integration

Once collision between two bodies is confirmed by the collision detection algorithm, the equations of motion are integrated to obtain the dynamic response of the two bodies. If the two bodies are made of different materials, their energetic restitution coefficients (CRSTRNG(m) in Appendix A) can be different. In this case, the minimum value is chosen for the restitution coefficient of this collision. The friction coefficient is determined in the same way. The procedures for collision integration are:

1) Calculate $[R]_{CB}$ and $[R]_{CS}$ using (36) and (37). Calculate $[J]_C$ using (35).
2) Calculate m_{ij}, $\overline{\mu}$ and $\overline{\phi}$ using equation (8) to (14).
3) If $\overline{\mu} \geq \mu$, solve $h(\mu, \hat{\phi}) = 0$ and $g(\mu, \hat{\phi}) > 0$ for $\hat{\phi}$ (equations (20) and (21)).
4) Estimate the total normal impulse of collision and select a small impulse increment Δp for the numerical integration (for example, Δp =1% of the estimated total normal impulse).
5) Set p=0 and W_3=0.

6) Calculate s and ϕ using (15) and (16) if collision is in the first phase of sliding. If it in the second phase of sliding, then $s=0$ and ϕ is a constant, $\phi=\hat{\phi}$. Ignore this step if it is in the slip-stick phase.
7) Increase p to $p+\Delta p$.
8) For the first and the second phases of sliding, use (17) to (19) to calculate v_1, v_2, v_3 as functions of p; for the slip-stick phase, integrate (26) to (28) for v_1, v_2 and v_3.
9) Integrate (4) to calculate p_1 and p_2 if collision is in the first or second phase of sliding. Use (23) to calculate p_1 and p_2 if it is in the slip-stick phase. Note $\phi = \hat{\phi}$ for the second phase of sliding.
10) Integrate W_3 using (6).
11) If collision is in the compression stage, check if maximum compression has been obtained (i.e., v_3 changes from negative to positive). If yes, then compression ends and restitution begins, $p_c = p$, and $W_3(p_c) = W_3$. Ignore this step if it is in restitution already.
12) If collision is in the restitution stage, check if Stronge's hypothesis in (5) is satisfied. If yes, then collision is completed with $p_f = p$. Go back to step 6) if Stronge's hypothesis is not satisfied or collision is in compression stage.
13) Obtain the total impulse $\vec{p}$ using equation (31). Use (29) and (30) to calculate mass center velocity and angular velocity at the end of the collision for both objects. Note that the impulses on the two objects are equal in magnitude and opposite in direction.

4. Application and Validation

In this section the collision model is illustrated by its application to several cases. Validation is made for a few simple tests through comparison of the computational results with the analytical and experimental results.

4.1. Central collision of two identical spheres

A central collision means that the mass centers of the two colliding bodies and the collision point are along the same line. Consider two identical iron spheres of 4.0 cm radius having a central collision. As shown in Figure 2, a moving sphere (on the left) approaches a stationary sphere (on the right) at the speed of 1.0 m/s. The collision is assumed to be frictionless. The computation is 3-D with the total number of uniform mesh cells 40×20×20. Computational results in the plane of symmetry are shown in Figure 1(a), (b) and (c) for three cases: purely elastic, completely plastic and partially elastic collisions. Calculated velocities of the two bodies at the end of collision are shown in Table 1. The corresponding analytical solutions can be obtained by solving equations of motion as

$$u_1 = \frac{1}{2}(1-e_*)u_{1,0} + \frac{1}{2}(1+e_*)u_{2,0}$$

$$u_2 = \frac{1}{2}(1+e_*)u_{1,0} + \frac{1}{2}(1-e_*)u_{2,0}$$

Table 1. Calculated velocities after central collision for two identical spheres

	Purely Elastic (e=1.0)	Purely Plastic (e=0.0)	Partially Elastic (e=0.5)
Left Object	0.0	0.5	0.25
Right Object	1.0	0.5	0.75

where $u_{1,0}$ and $u_{2,0}$ represent the velocities of the two objects before the collision, respectively. In this case, object 1 is the object at left and object 2 is at right. $u_{1,0}$ and $u_{2,0}$ are 1.0 and 0.0 respectively. It is found that the computational and analytical results match each other exactly.

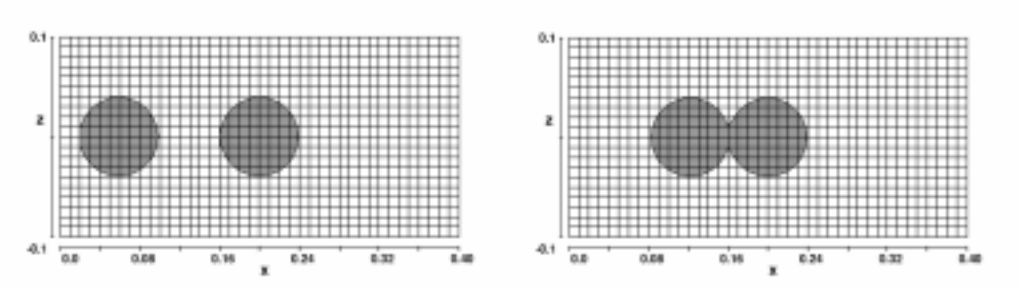

t = 0.009 s t = 0.072 s

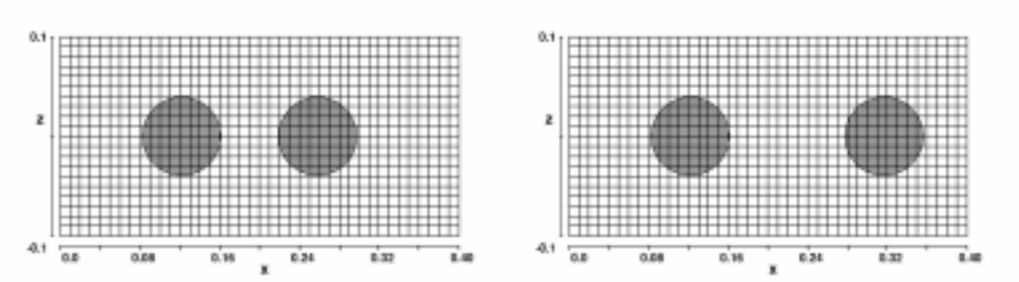

t = 0.1305 s t = 0.189 s

(a) purely elastic (e*=1.0)

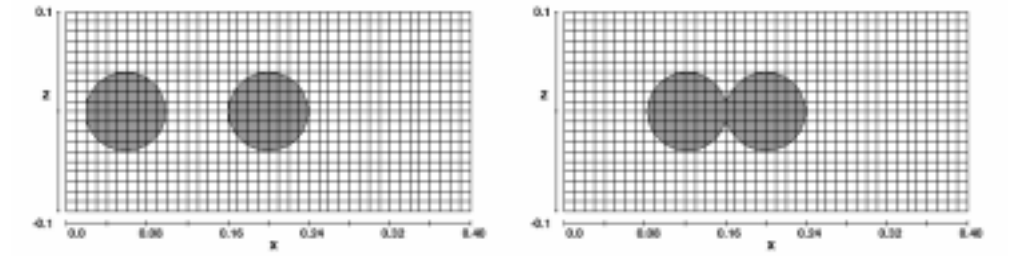

t = 0.009 s t = 0.072 s

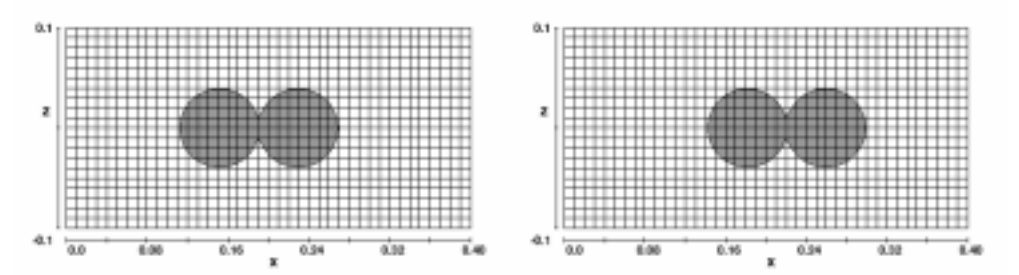

t = 0.1305 s t = 0.189 s

(b) purely plastic (e*=0.0)

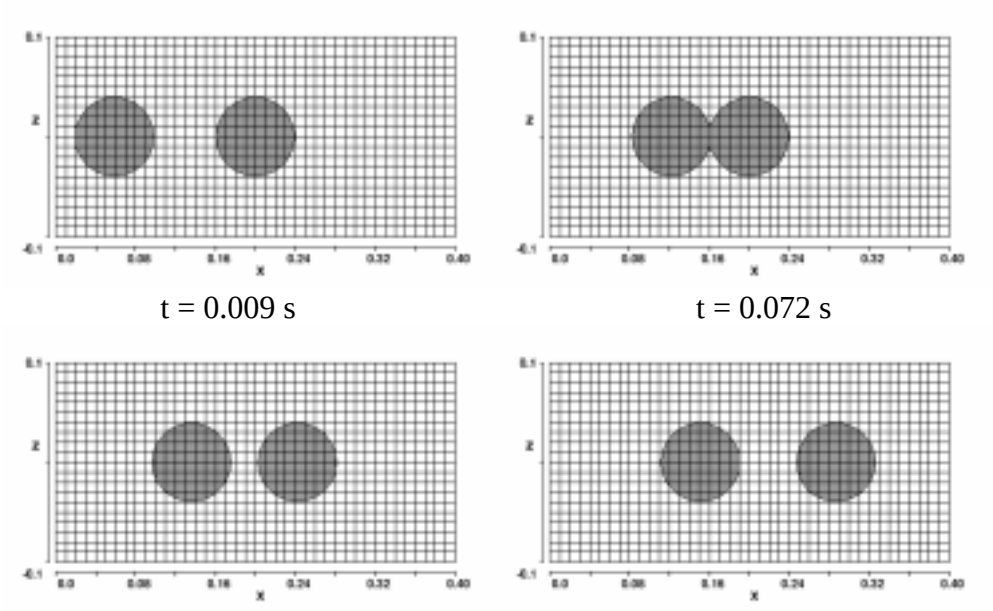

t = 0.009 s t = 0.072 s

t = 0.1305 s t = 0.189 s

(c) partially elastic

Figure 2. Central collision of two identical spheres, (a) purely elastic collision, (b) purely plastic collision, (c) partially elastic collision.

4.2 A Sphere Dropping onto a Level Anvil

Consider a sphere dropping onto a level anvil from height h_0 at time t_0. 3-D computation is conducted for h_0=0.5m and e=0.8 for a sphere of radius 10 cm. The height and upward velocity of the sphere versus time obtained by computation are shown in Figures 3 and 4, respectively. Analytical solutions of the rebound height h_i after i number of bounces and the corresponding time t_i are (Stronge, 2000)

$$h_i = e^{2i} h_0 \qquad t_i = \sqrt{\frac{2h_0}{g}}\left(-1 - e^i + 2\sum_{j=0}^{i} e_*^j\right)$$

Table 2 shows comparison of the computational result with the analytical solution for h_i and t_i. It is seen that the computational result matches the analytical solution with a high degree of accuracy.

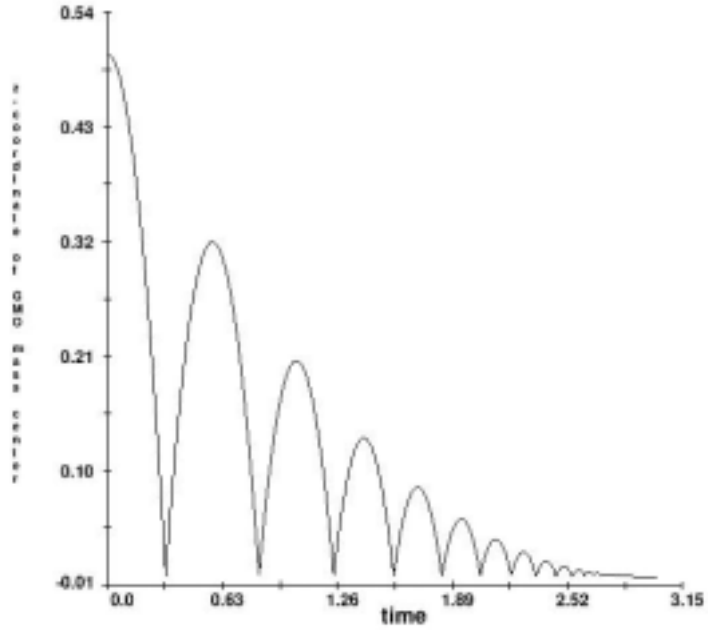

Figure 3. Calculated height of the sphere versus time

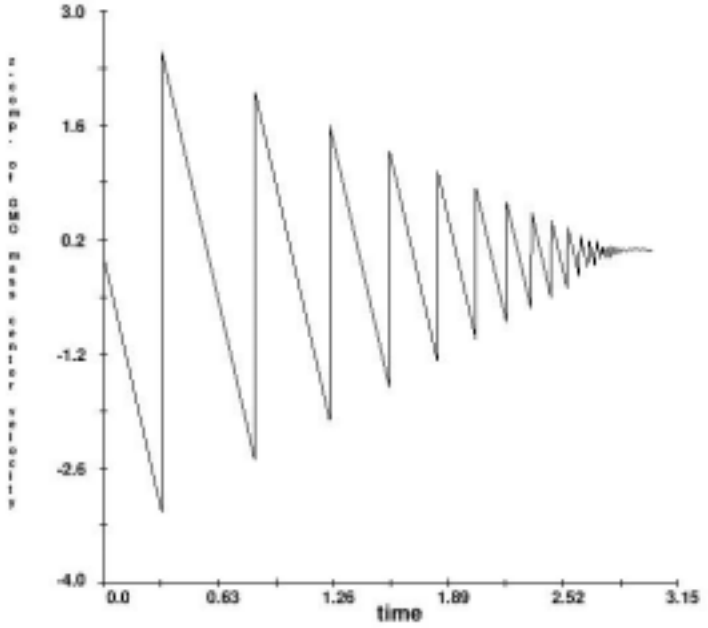

Figure 4. Calculated vertical velocity of the sphere versus time

Table 2. Computational and analytical solutions for the rebound height h_i after i number of bounces. t_i is the corresponding time

i	t_i		h_i	
	Computation	Analytical	Computation	Analytical
1	0.57338488	0.5750	0.31968856	0.3200
2	1.0332109	1.0345	0.20558004	0.2048
3	1.4089241	1.4030	0.13137612	0.1311
4	1.6995362	1.6974	0.084260948	0.08389
5	1.9363257	1.9329	0.053757090	0.05368
6	2.1268764	2.1213	0.034258254	0.03436
7	2.2786703	2.2720	0.021794900	0.021999
8	2.4056954	2.3926	0.013392366	0.014074
9	2.5059292	2.4891	0.0079711881	0.009007

4.3 Pool Ball Break

Figure 5 shows the result of a 3-D simulation for pool ball break. Initially all adjacent balls in the rack contact each other. Elastic collision is assumed with e =1.0. The balls collide with each other and also with the wall and the surface of the table. Micro-collisions occur between the balls and the table surface, preventing the balls from penetrating into the table. The results look reasonable according to the common experience, but no experimental results are found for comparison.

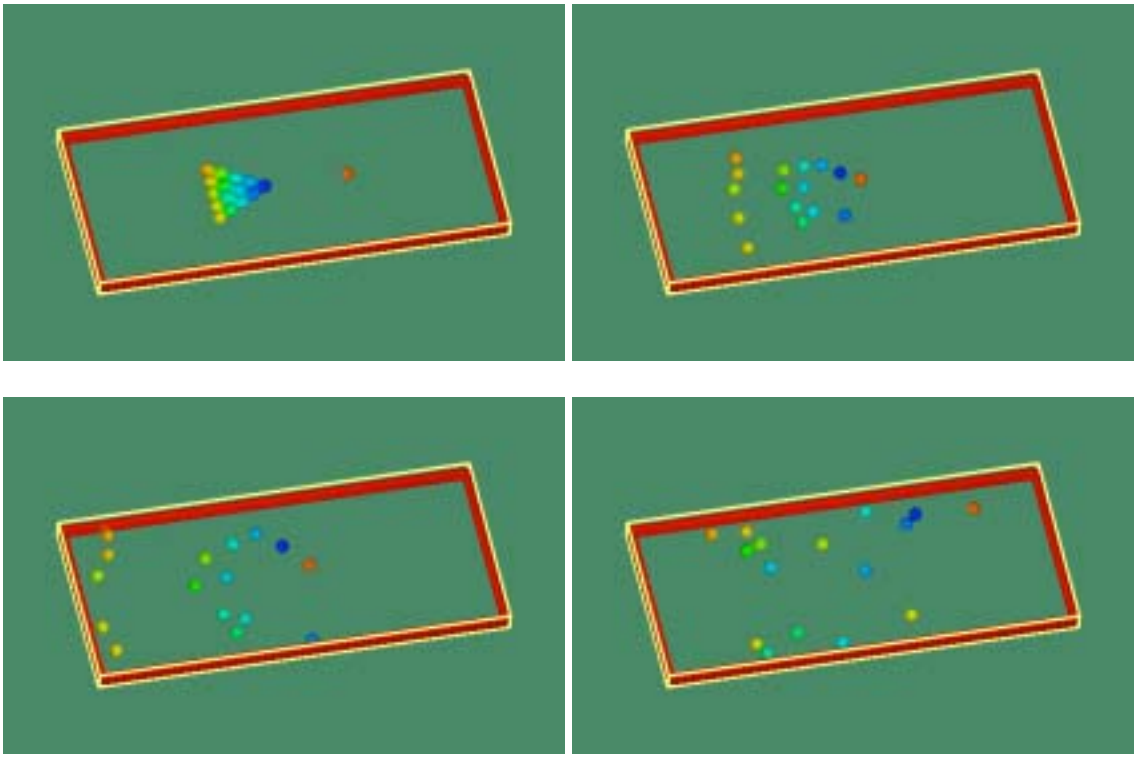

Figure 5. Computational result of pool break

4.4 Domino Toppling

Consider an evenly spaced array of uniformly slender blocks that initially stand on a rough level surface. The height of each block is 4.178 cm, the width (in the lateral direction of the array) is 2.19 cm, and the thickness (in the direction along the array) is 0.758 cm. Space between two neighbor blocks is 2.191 cm. 3-D simulation of Domino toppling of the block array was conducted using the collision model. The energetic restitution coefficient is 0.846. Friction coefficient is 0.176. Figure 6 displays the computational result and high speed film frames (Stronge, 2000) in pairs. Each pair is selected with the closest configuration with the time of the first pair set at zero. Comparison shows a good agreement between the calculated time and the measured time for these pairs of graphs. For the speed of the toppling wave front, its calculated value is 98.96 cm/s, matching quite closely with the measured value of 104.0 cm/s.

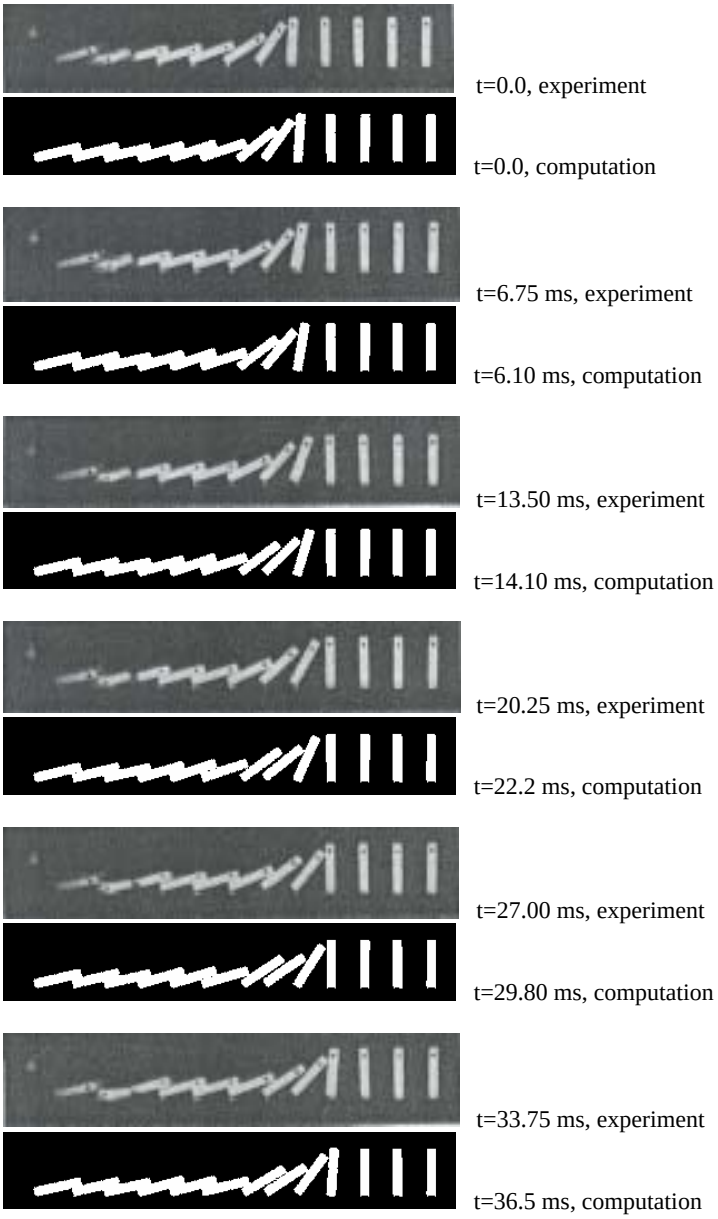

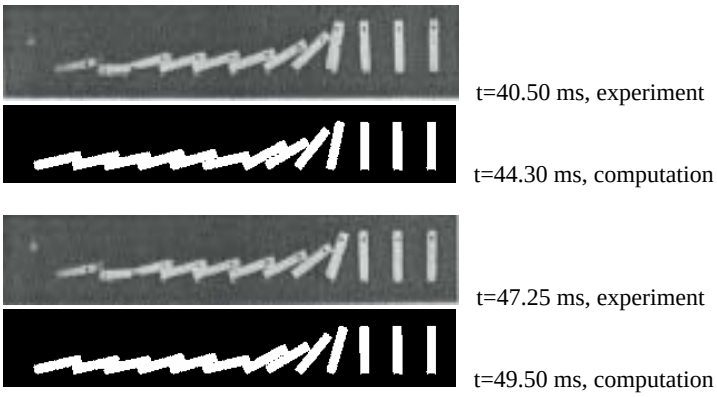

Figure 6. Comparison of computational result and frames of high speed film

4.5 Flushing of a Solid Sphere in Toilet

Computation for a toilet flushing problem is conducted to demonstrate the capability of the collision model when fluid flow is present. A sphere of 4.2 cm diameter is initially located at the bottom of the toilet container, as shown in Figure 7(a). Its mass density is 1.17 g/cm^3. The collision model is activated for plastic collision (energetic restitution coefficient is 0.0) with frictional coefficient to be 0.1. The total simulation time is 5.5 sec. Figures 7(b) to (h) present the sphere locations at different times from t=0 to t=0.149 sec. Many collisions of the sphere against the toilet bottom/wall and the duct wall occur. The sphere's motion during flushing is determined by the total effect of these collisions, the hydraulic force and gravitational force. The computation was conducted using a Pentium 3.0 Ghz PC with 2.0 GB of memory. The total number of cells in the mesh was 2.5 million. Simulation time was 5.5 sec, and 83.3 hours of CPU time was required to complete the run.

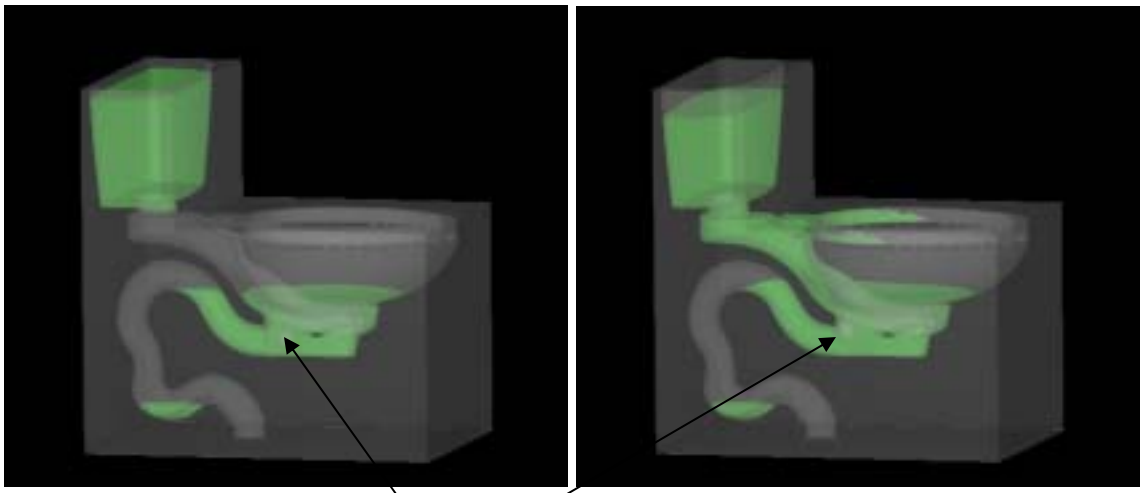

(a) t=0 (b) t=0.044 sec

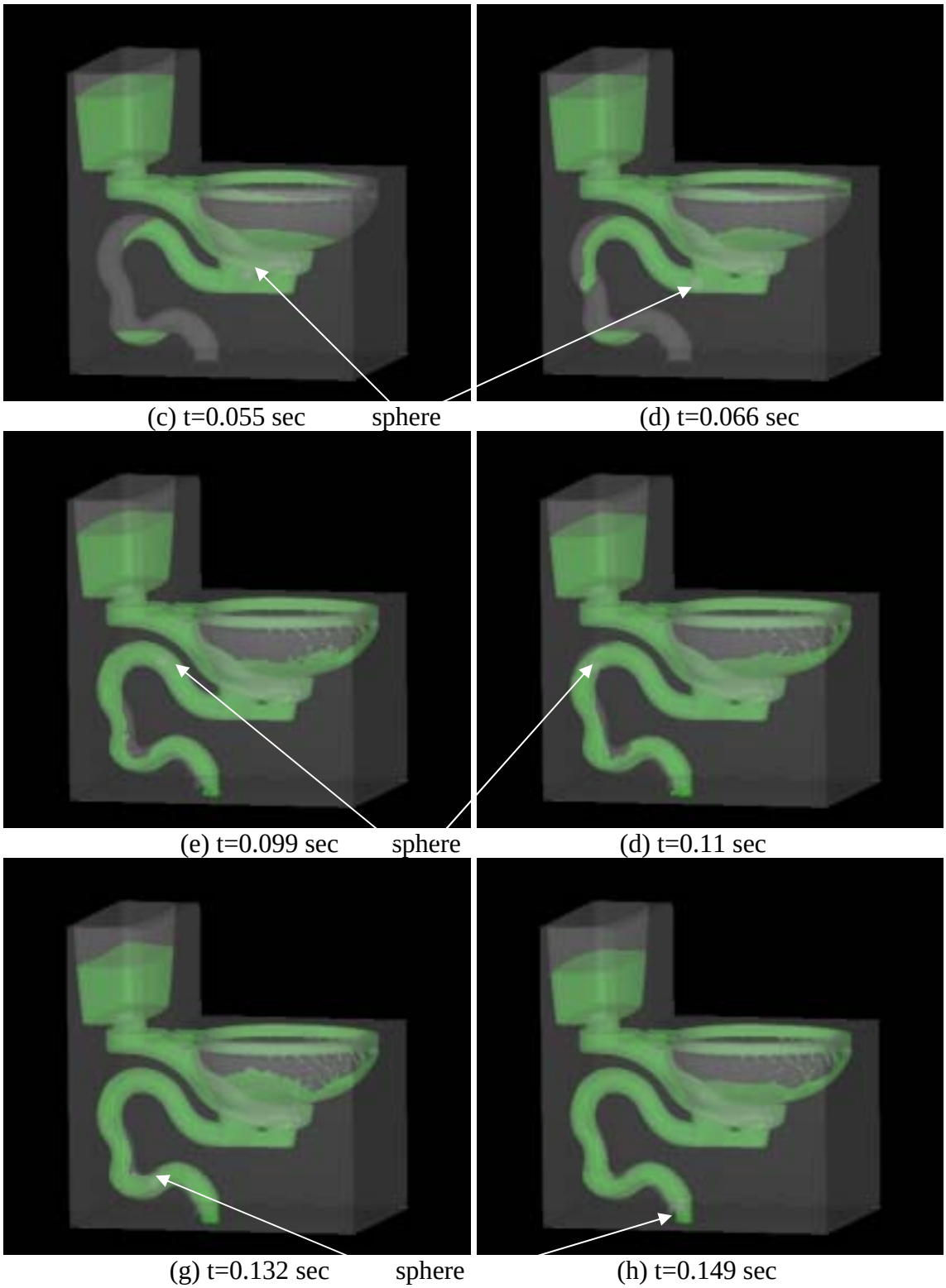

Figure 7. Computational result of flushing of a sphere in toilet

4.5 Drifting of Logs in Water Stream

A problem for drifting logs in a water stream was simulated. The computational domain includes a reservoir and a channel which are connected to each other at the gate of the reservoir. The reservoir is 6.5 m deep, 15.0 m long (in the direction of the channel) and 18.0 m wide. The gate has a step of 1.5 m high from the channel bottom. Initially there are 5 wood logs of 6.0 m length, 1.0 m diameter and 500 kg/m^3 density floating in the still water of the reservoir. At time t=0, the gate is instantly opened and the wooden logs start moving to the gate due the motion of water. Figure 8 shows log positions at different stages of the process. In Figure 8(b) and (c), two logs move toward the channel by sliding along the wall of the gate. In Figure 8(d), the two logs collide on the step of the gate when they are drifted into the channel by the waterfall. In Figure 8(e), the two logs contact each other while moving downstream in the channel. In Figure 8(f), another log collides on both the step of the gate and the bottom of the channel, when entering the channel. Figures 8(g) to (l) show the motion of the last log when it goes through the gate into the channel. The right end of log hits the wall first (Figure 8(g)) and the right end follows (Figure 8(h)), causing a temporary jamming of the log before the gate. Note that the log is located more to the left of the center line of the gate. The fast stream through the gate thus results in a lower pressure under the log at its right end than at the left end. This makes the log turn down its right end and pass through the gate. During the whole drifting process, there are a lot of collisions of the logs with walls and the step of the gate as well as with the bottom of the channel. In this computation, the energetic restitution coefficient e is 0.632, and friction coefficient μ is 0.1. Due to the comparatively low mass density of the wood (50% that of water), a newly developed implicit GMO method was used to stabilize the computation. The total number of computational cells was 700,000. Simulation time is 1.0 min. The computation was conducted with a Pentium 3.0 Ghz PC with 2.0 GB of memory. The CPU time was 45 hours and 12 minutes.

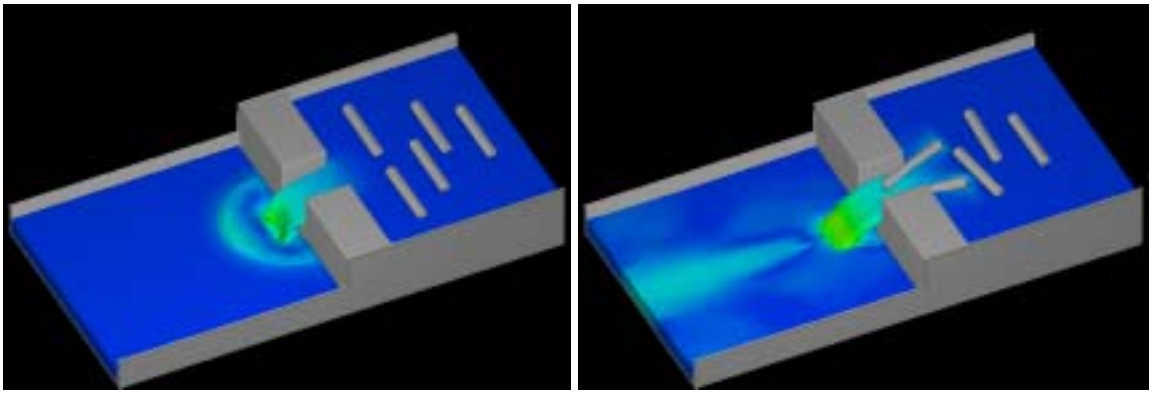

(a) (b)

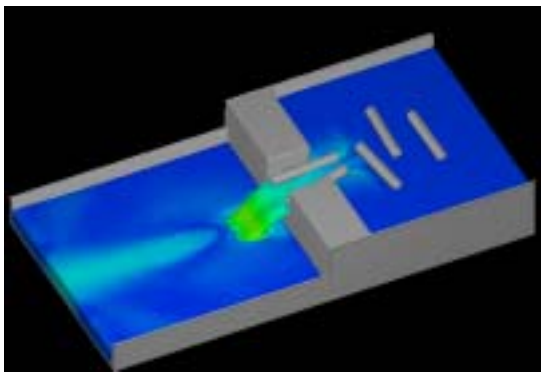

(c)

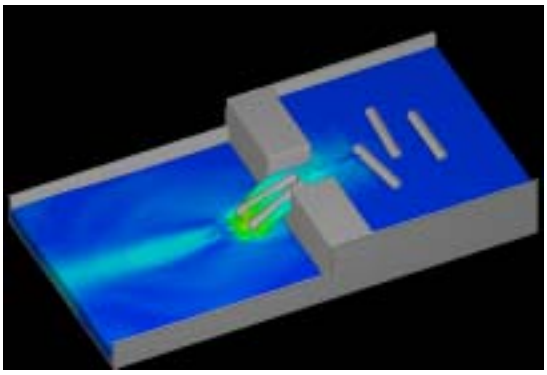

(d)

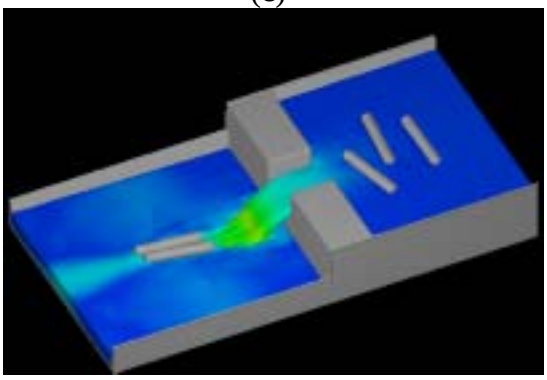

(e)

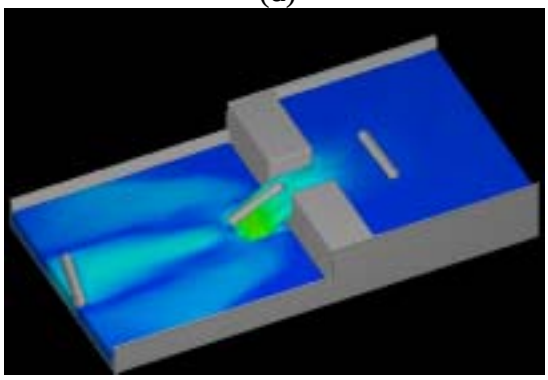

(f)

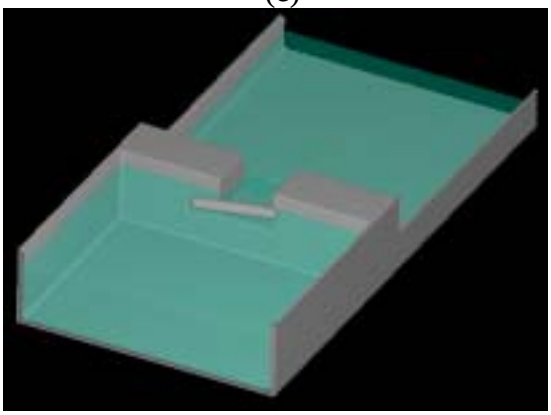

(g)

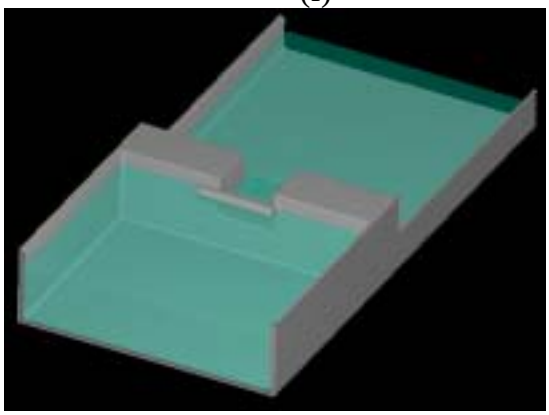

(h)

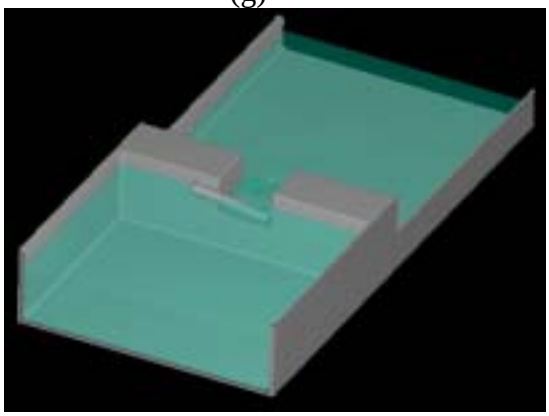

(i)

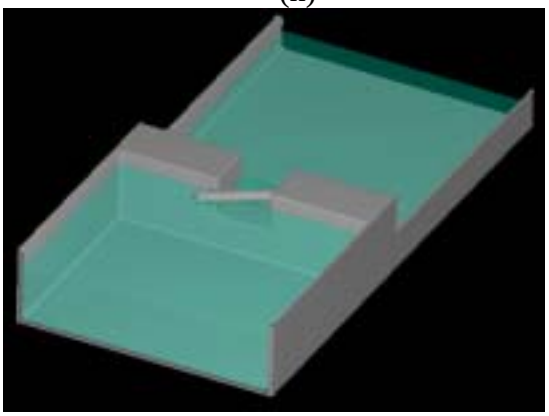

(j)

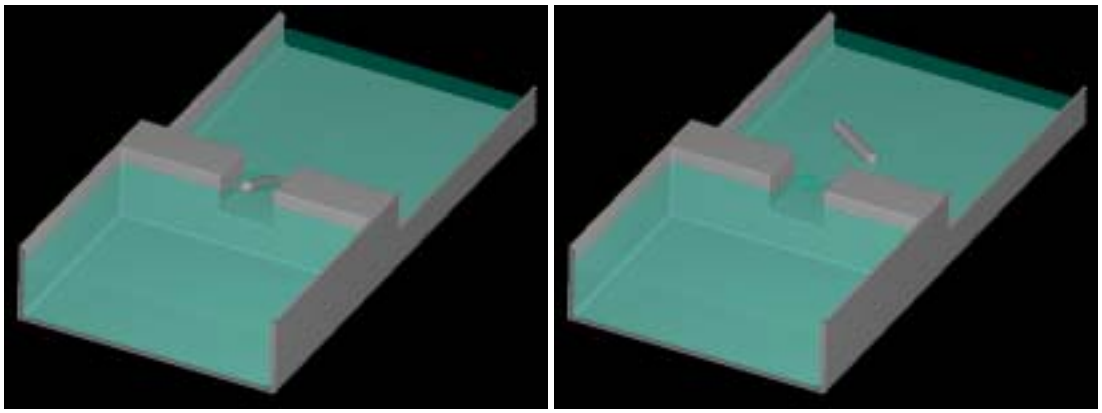

(k) (l)

Figure 8. Computed result for drifting of wood logs by water. Color in (a-f) represents fluid velocity.

4.7 Stones Driven by Water Stream

Using the new collision model, a simulation of stone motion driven by water stream in a stepped channel was conducted. As shown in Figure 9(a), 23 marble stones initially set still on bottom of a channel, which include 8 spheres of 0.3m diameter and 15 bricks with dimensions of 0.25m×0.3m×0.6m. The computational domain is 9.5 m long, 4.0 m wide and 2.0 m high. The energetic restitution coefficient and the friction coefficient are assumed to be 0.9 and 0.1, respectively. From time t=0, water at the 3 m/s boundary velocity floods the channel. Figure 9 shows calculated stone locations at different times. Before water reaches the stones, the stones sit on the channel bottom through a series of micro-collisions. These collisions are hardly seen although they can be observed from printed values of the stone velocities. Once water hits the stones, the stones experienced lots of strong collisions between each other and with the channel bottom. The collisions are especially strong when the stones fall over the two steps and hit the bottom of the channel. The motion of each stone is the result of the combined effect of the collision impact, the hydraulic force and the gravitational force. In this computation, the total number of mesh cells was 544,000. Simulation time is 3.5 sec. The computation was conducted using a Pentium 3.0 Ghz PC with 2.0 GB of memory. The CPU time was 10.56 hours.

5. Conclusions

In this work the capability to simulate rigid body collision was developed and implemented for ***FLOW-3D***® as an addition of the general moving object model. The basic model of Stronge (2000) for rigid body collision with 6-DOF was adopted and further developed for two more cases: 1) bodies with fixed axis/point, 2) in a pair of colliding bodies one has prescribed motion and the other has coupled motion. Algorithms for collision detection and collision integration were also developed and implemented. The new model was applied to several cases with or without presence of fluid flow. Reasonable results and good agreement with analytical and experimental results were obtained.

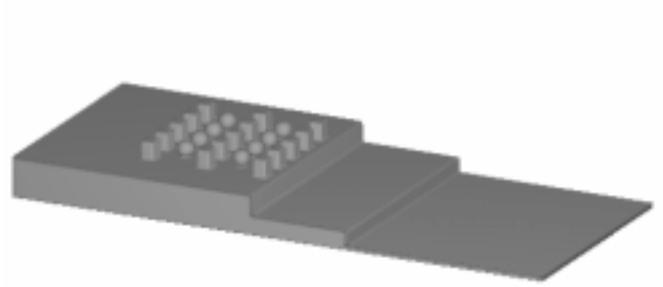

(a) t=0.0 sec

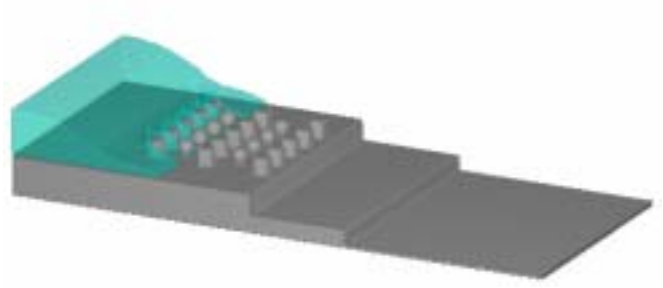

(b) t=0.5 sec

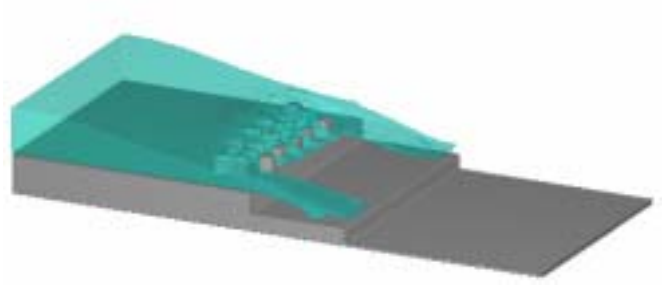

(c) t=1.0 sec

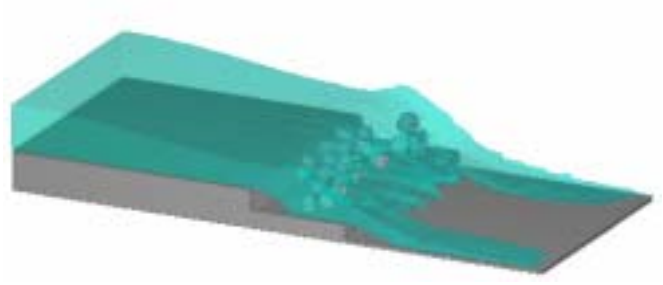

(d) t=1.5 sec

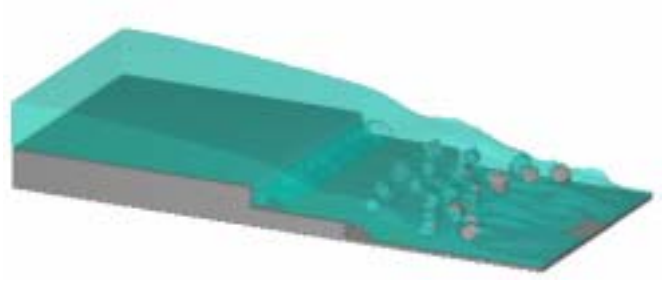

(e) t=2.0 sec

Figure 9. Stones driven by water stream in a channel

References

Barkhudarov, M. B., Wei, G. 2006, Modeling of the Coupled Motion of Rigid Bodies in Liquid Metal, MCWASP 2006, Opio, France.

Kelly, J. B. 1986, Impact with Friction. Journal of Applied Mechanics, Vol. 53/1, 1986.

Mirtich, B. V. 1996, Impulse-based Dynamics Simulation of Rigid Body System. PhD thesis, University of California, Berkeley.

Stronge, W. J. 2000, Impact Mechanics. Cambridge University Press, Cambridge, UK.

Wei, G. 2005a, A Fixed-Mesh Method for General Moving Objects, Flow Science Technical Note (FSI-05-TN73).

Wei, G., 2005b, A Fixed-Mesh Method for General Moving Objects in Fluid Flow, Modern Physics Letters B, Vol. 19, Nos. 28-29, 1719-1722.

Appendix A. Input Parameters

Namelist XPUT

VARIABLE	DEFAULT	DESCRIPTION
ICLID	0	Flag for collision model activation =0, do not activate collision model =1, activate collision model.
STRNGMOB	1.0	Global value of Stronge's energetic restitution for collision.
FRCMOB	0.0	Global value of friction coefficient for collision

Namelist OBS

m, n ≤ 500, obstacle index

VARIABLE	DEFAULT	DESCRIPTION
CRSTRNG(m)	STRNGMOB	Stronge's energetic restitution coefficient for collision.
CFRC(m)	FRCMOB	Friction coefficient for collision
ICLIDOB(m,n)	ICLID	Flag for collision between object m and n =0, collision is not allowed between objects m and n =1, collision is allowed between objects m and n. Note: if iclid(m,m)=0, then collision is not allowed for object m with any other objects and domain boundaries.